Full Length Research Paper

Two-dimensional simulation of flow pattern around a groyne using semi-implicit semi-Lagrangian method

Hamed Sarveram[1]*, Abolfazl Shamsai[1] and Mohammad Ali Banihashemi[2]

[1]Department of Civil Engineering, Science and Research Branch, Islamic Azad University, Tehran, Iran.
[2]School of Civil Engineering, College of Engineering, University of Tehran, Iran.

In this article, a numerical model was obtained in a two dimensional flow pattern simulation around a groyne. The model approximates the depth-averaged, shallow water equations with a finite volume, semi-implicit and semi-Lagrangian representation. Runge-Kutta scheme was used for departure point determination. The results showed that numerical model has high stability and efficiency. Also, numerical representation has the ability to recognize land boundaries; therefore, closed boundaries do not need specification. The comparison between numerical formulation results and experimental results show that except in areas with strong downward flow, there are good agreements between experimental and calculated results.

Key words: Semi-Lagrangian, semi-implicit, shallow water, flow pattern, groyne.

INTRODUCTION

In hydraulics and coastal engineering, groynes (Figure 1) are very important structures for river navigation and coastal protection. Many experimental and numerical researches have been done in order to examine flow pattern and scouring around groynes. These studies were carried out in different conditions in terms of groyne length, groyne installation angle towards the approaching flow, permeable or impermeable states, submerged and non-submerged states and number of groynes (Yeo et al., 2005), etc. Powerful software such as FLUENT, FLOW3D have been a great help to develop these simulations (Shahrokhi and Sarveram, 2011; Abbasi et al., 2011). Despite the large amount and variety of researches that have been carried out so far in this field, no comprehensive and well-organized response has been provided yet. However considerable differences can be seen between the research results.

The groyne which is located at the river main flow, perpendicularly causes narrowing and deviation of the flow and this in turn gives a complex three dimensional form to flow around a groyne. As local scouring, sediment transport and settlement around groyne require clarifying the three-dimensional flow pattern. It is necessary to consider the flow pattern around a groyne, which is important and necessary to conduct experimental examinations. However, for a full understanding of this flow pattern, one has to use numerical techniques.

The first research in this field was carried out by Francis et al. (1968). They considered separation zone for various types of groyne in a rectangular flume, but they did not measure the flow velocities. Researches done by Rajaratnam and Nwachukwu (1983), however, contain velocity measurements in the flow field. Ettema and Muste (2004) examined the effect of groyne length on downstream separation region by considering the effect of scale. Researches by Yeo et al. (2005) also deal with an experimental examination of the downstream separation region of a groyne under various groyne lengths, various installation angles and various degrees of groyne permeability.

Tingsanchali and Maheswaran (1990) used a two-dimensional depth-averaged model, incorporating a correction factor used in the k–ε model and introducing a three-dimensional correction factor to improve the computed bottom stresses. Molls et al. (1995) also developed a general mathematic model to solve the unsteady two-dimensional depth averaged equations by combining it with a constant eddy viscosity turbulent

---

*Corresponding author. E-mail: hamed.sarveram@gmail.com.
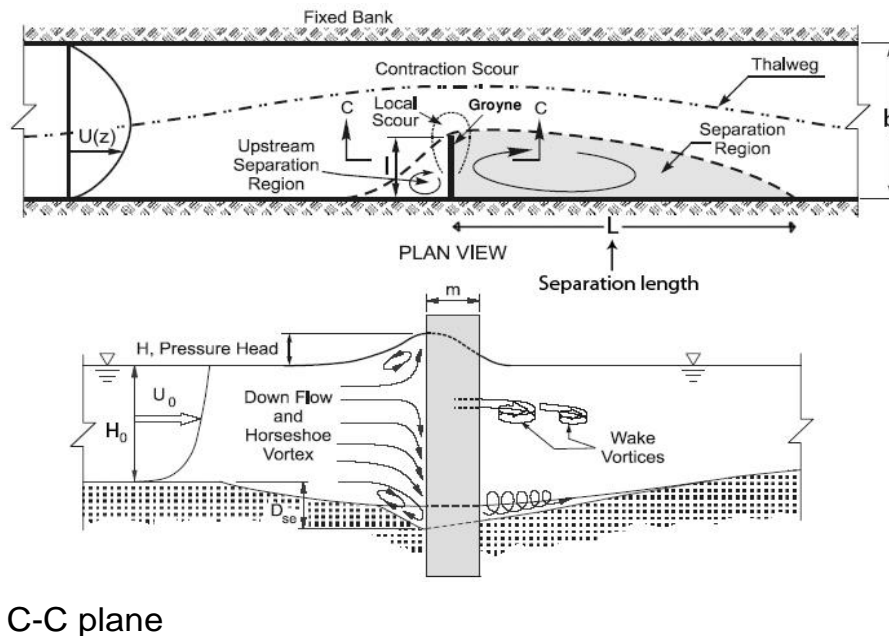
C-C plane

Figure 1. Schematic model of groyne-surrounding flow.

model. A great deal of research has been carried out in recent years, especially by Chinese researchers such as Zhanfeng and Xiaofeng (2006), Quanhong and Pengzhi (2007) and Tang and Ding (2007). They studied the model and scouring around groyne by using various models of Turbulence under different conditions of flow and groyne dimension.

Mathematical descriptions of fluid flow are divided into two groups: Eulerian and Lagrangian. Eulerian describes the flow within a single fixed reference frame, through which the fluid flows. The second description happens within the fluid, which is known as Lagrangian. Here the observer is moving with the fluid.

In fact any numerical model which we make inevitably has limitations. One of these failures in flux based Eulerian scheme is the difficulty of achieving stable and accurate simulations with long time steps. For a fluid which moves across several cells in a single step with sufficiently long time steps, the flux transfers between cells becomes extremely difficult to show (Leonard, 1993). In practice, schemes of this form are operated such that only flows between each cell and its immediate neighbors need to be considered during any single time-step. If the scheme is explicit, this constraint becomes a necessary condition for stability. Lagrangian schemes operate with a far less severe restriction on the time-step length, especially where the flow is strongly advection dominated. For such flows, the Lagrangian forms of the evolution equations are more tractable numerically than the equations in Eulerian form. As a result, the time step can substantially increase beyond what would be acceptable for an Eulerian scheme, without detriment in either stability or accuracy. However, Lagrangian numerical

schemes are still methods of approximation and as such subject to limitations of some kind or others. The basic particle–trajectory model invariably falls foul of the profusion of scales which are typical in any realistic fluid flow. An initially evenly distributed collection of particles may, with time, become broken up into clusters and voids. The consequence of this is a loss of model representation for the fluid as a whole.

Semi-Lagrangian methods attempts to retain the desirable properties of the two descriptions by avoiding their less desirable failures and by integrating along particle trajectories while, evaluating target functions at mesh points at every time step. For a review on primary semi-Lagrangian schemes and related issues see Staiforth and Cote (1991).

This paper is organized as follows: first, the governing equations (shallow water equations) are presented; second, presents the numerical formulation of the purposed model; and finally, the results of the numerical applications for two-dimensional cases of flow pattern around a groyne were obtained.

GOVERNING EQUATIONS

The governing equations are the depth-averaged, shallow water equations. These equations assume a hydrostatic pressure distribution, a well mixed water column, and a small depth to width ratio.

$$\frac{\partial U}{\partial t} + U\frac{\partial U}{\partial x} + V\frac{\partial U}{\partial y} = -g\frac{\partial \eta}{\partial x} + \varepsilon\left(\frac{\partial^2 U}{\partial x^2} + \frac{\partial^2 U}{\partial y^2}\right) - g\frac{n^2\sqrt{U^2+V^2}}{H^{4/3}}U \quad (1)$$

$$\frac{\partial V}{\partial t} + V\frac{\partial V}{\partial y} + U\frac{\partial V}{\partial x} = -g\frac{\partial \eta}{\partial y} + \varepsilon\left(\frac{\partial^2 V}{\partial x^2} + \frac{\partial^2 V}{\partial y^2}\right) - g\frac{n^2\sqrt{U^2+V^2}}{H^{4/3}}V \qquad (2)$$

$$\frac{\partial \eta}{\partial t} + \frac{\partial (HU)}{\partial x} + \frac{\partial (HV)}{\partial y} = 0 \qquad (3)$$

Where U is the depth-averaged in x-direction velocity component, V is the depth averaged y-direction velocity component, η is the free surface elevation, g is the gravitational constant, t is time, ε is the horizontal eddy viscosity coefficient, H is the total water depth, h is undistrubed water depth, n is Manning's roughness coefficient, as shown in the Figure 2, $H = \eta + h$.

NUMERICAL MODELING

As shown in Figure 2, free surface elevation, η, is defined at the center of each computational volume. Total water depth, H, and directional velocity components, U and V, are defined at the midpoint of volume faces. Undisturbed water depth, h, is also defined at the midpoint of volume faces. The finite volume structure provides a control volume representation that is inherently mass conservative (Clive, 1991).

The combination of a semi-implicit free surface solution and a semi-Lagrangian representation of advection, provide advantages of a stable solution. In the semi-implicit process, the free surface elevation in the momentum equations (that is, Equations 1 and 2), and the velocity divergence in the continuity Equation 3, is treated implicitly. The advective terms in the momentum equations are discretized explicitly. When the explicitly
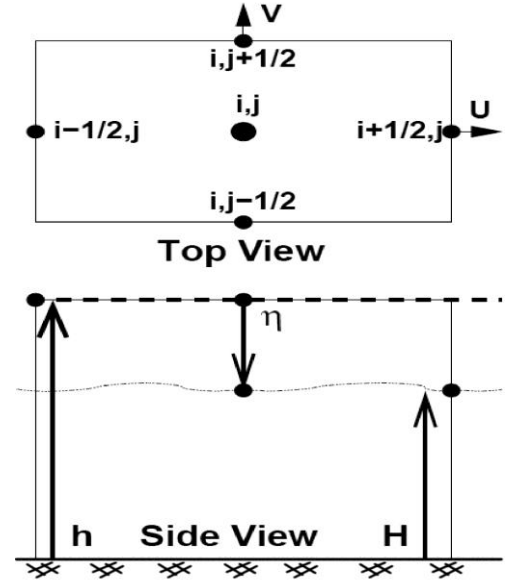

Figure 2. Location and variable definition of flow on computational grid.

discretized advection terms are represented with a semi-Lagrangian approach, researches show that the Courant number stability condition on time step duration could be relaxed (Vicenzo, 1990). Additionally, Robert (1982) demonstrated that the association of a semi-Lagrangian treatment of advection and a semi-implicit representation of gravitational oscillations provides a six-fold increase in the maximum stable time step duration in atmospheric modeling.

The continuity equation is discretized as follows:

$$\eta_{i,j}^{N+1} = \eta_{i,j}^{N} - \theta\frac{\Delta t}{\Delta x}\left(H_{i+1/2,j}^{N}U_{i+1/2,j}^{N+1} - H_{i-1/2,j}^{N}U_{i-1/2,j}^{N+1}\right) - \theta\frac{\Delta t}{\Delta y}\left(H_{i,j+1/2}^{N}V_{i,j+1/2}^{N+1} - H_{i,j-1/2}^{N}V_{i,j-1/2}^{N+1}\right)$$

$$-(1-\theta)\frac{\Delta t}{\Delta x}\left(H_{i+1/2,j}^{N}U_{i+1/2,j}^{N} - H_{i-1/2,j}^{N}U_{i-1/2,j}^{N}\right) - (1-\theta)\frac{\Delta t}{\Delta y}\left(H_{i,j+1/2}^{N}V_{i,j+1/2}^{N} - H_{i,j-1/2}^{N}V_{i,j-1/2}^{N}\right) \qquad (4)$$

Where (i, j) subscript is spatial location and the superscript, N or N+1, represents the temporal location, Δx and Δy represent the x and y direction volume lengths respectively, Δt is the computational time step duration, θ represents the degree of implicitness. Researches show that an implicit or semi-implicit free surface elevation solution provides enhanced stability (Robert, 1982; Vicenzo, 1990).

The numerical approximations with conservation of momentum equations, give the following equations:

$$U_{i+1/2,j}^{N+1} = FU_{i+1/2,j}^{N} - (1-\theta)\frac{g\Delta t}{\Delta x}\left(\eta_{i+1,j}^{N} - \eta_{i,j}^{N}\right) - \theta\frac{g\Delta t}{\Delta x}\left(\eta_{i+1,j}^{N+1} - \eta_{i,j}^{N+1}\right)$$

$$-g\Delta t\frac{n_{i,j}\left[\left(U_{i+1/2,j}^{N}\right)^2 + \left(V_{i+1/2,j}^{N}\right)^2\right]^{0.5}}{\left(H_{i+1/2,j}^{N}\right)^{4/3}}U_{i+1/2,j}^{N+1} \qquad (5)$$

$$V_{i,j+1/2}^{N+1} = FV_{i,j+1/2}^{N} - (1-\theta)\frac{g\Delta t}{\Delta y}\left(\eta_{i,j+1}^{N} - \eta_{i,j}^{N}\right) - \theta\frac{g\Delta t}{\Delta y}\left(\eta_{i,j+1}^{N+1} - \eta_{i,j}^{N+1}\right)$$

$$-g\Delta t\frac{n_{i,j}\left[\left(U_{i,j+1/2}^{N}\right)^2 + \left(V_{i,j+1/2}^{N}\right)^2\right]^{0.5}}{\left(H_{i,j+1/2}^{N}\right)^{4/3}}V_{i,j+1/2}^{N+1} + \Delta t\frac{\gamma_T\left(V_a - V_{i,j+1/2}^{N+1}\right)}{H_{i,j+1/2}^{N}} \qquad (6)$$

Where, the FU and FV terms are the semi-Lagrangian advection operators. A semi-Lagrangian advection method employs a Lagrangian algorithm across the underlying Eulerian model grid. The Lagrangian component of the scheme traces the path line of a particle which is initially located at the volume face, which is the velocity definition location from Figure 1. Going backwards along the particle path lie a distance

corresponding to the simulation time step duration (Δt) obtained. The particle departure point is the location of the particle at the beginning of the current time step. Again, this location is obtained by tracing the particle

backwards along the path line (Bermejo, 1990). The method is only semi-Lagrangian, and partially Eulerian, because the velocity value at the departure point is obtained by interpolation from the surrounding known velocity values defined on the Eulerian grid.

$$FU_{i+1/2,j}^{N} = U_{sL_{bicubic}}^{N} + \varepsilon \Delta t \left(\frac{U_{i+1/2-a+1,j-b}^{N} - 2U_{i+1/2-a,j-b}^{N} + U_{i+1/2-a-1,j-b}^{N}}{\Delta x^2} \right) \qquad (7)$$

$$FV_{i,j+1/2}^{N} = V_{sL_{bicubic}}^{N} + \varepsilon \Delta t \left(\frac{V_{i-a+1,j+1/2-b}^{N} - 2V_{i-a,j+1/2-b}^{N} + U_{i-a-1,j+1/2-b}^{N}}{\Delta x^2} \right) \qquad (8)$$

In Equation 7 and 8, the subscript sL$_{bicubic}$ denotes bicubic interpolation from the underlying Eulerian grid at the departure point. In the viscous terms, ε is the horizontal eddy viscosity which is set as a fixed value. The subscripts on the velocity terms in the viscous terms denote the location on the Eulerian grid relative to the departure point (i + 1/2 - a; j - b) in Equation 8, where a (a = U Δt/Δx), is the x-direction Courant number rounded down and b (b = V Δt/Δy), is the y-direction Courant number rounded down.

In this article, fourth-order, four-step, explicit Runge-Kutta schemes (Chunmiao and Bennett, 1995) have been used for departure point determination. In this method, the partial time step (τ) is calculated with Equation 12, which enforces the Courant number criterion. The four step method in Equations 9 and 10 provides the particle location at the end of each partial time step. Each of the velocity values in these equations are obtained with bilinear interpolation from the underlying Eulerian grid, and the subscript b on the time level denotes bilinear interpolation. After M partial time steps, the particle has been traced backwards along the path line to locate the departure point. Each partial time step will move the particle no farther than one computational volume backwards because of the Courant number restriction contained in Equation 12.

$$x_{s-1} = x_s - \frac{\tau}{6}\left(U_{x_s,y_s}^{N_b} + 2U_{x_{sp1},y_{sp1}}^{N_b} + 2U_{x_{sp2},y_{sp2}}^{N_b} + U_{x_{sp3},y_{sp3}}^{N_b}\right) \quad (9)$$

$$x_{sp3} = x^s + U_{x_{sp2},y_{sp2}}^{N_b}\tau \quad x_{sp2} = x^s + U_{x_{sp1},y_{sp1}}^{N_b}\frac{\tau}{2}$$

$$x_{sp1} = x_s + U_{x_s,y_s}^{N_b}\frac{\tau}{2}$$

$$y_{s-1} = y_s - \frac{\tau}{6}\left(V_{x_s,y_s}^{N_b} + 2V_{x_{sp1},y_{sp1}}^{N_b} + 2V_{x_{sp2},y_{sp2}}^{N_b} + V_{x_{sp3},y_{sp3}}^{N_b}\right)$$
(10)

$$y_{sp3} = y_s + V_{x_{sp2},y_{sp2}}^{N_b}\tau \quad y_{sp2} = y_s + V_{x_{sp1},y_{sp1}}^{N_b}\frac{\tau}{2}$$

$$x_{sp1} = x_s + U_{x_s,y_s}^{N_b}\frac{\tau}{2}$$

$$s = M, M-1, M-2, ..., 2, 1 \qquad (11)$$

$$\tau \le \min\left[\frac{\Delta x}{\max_{i,j}|U|}, \frac{\Delta y}{\max_{i,j}|V|}\right] \qquad (12)$$

SOLUTION METHOD AND BOUNDARY CONDITIONS

Equation 4 has three unknowns, η^{N+1}, U^{N+1} and V^{N+1}. Substituting U^{N+1} and V^{N+1} respectively into Equations 5 and 6 would result to an equation which has only free surface elevations as the unknowns. Arranging the unknowns (N+1 terms) on the left side and the knowns (N terms) on the right side, provides the system of equations for free surface elevation. This system is penta-diagonal, positive definite and is solved with the preconditioned conjugate gradient method (Hestenes and Stiefel, 1952).

One advantage of proposed method is a natural and elegant treatment of wetting and drying boundaries on the underlying Eulerian grid. The finite volume layout in Figure 1 portrays an individual volume with total water depth (H) and undisturbed water depth (h) located at the volume faces. The free surface elevation for each volume (η) is defined at the volume center. Employing this layout, the total water depth across the simulation domain at each time step is updated with Equations 13 and 14.

The total water depth is the sum of the free surface elevation (η$_{i,j}^{N+1}$ or η$_{i+1,j}^{N+1}$) with the undisturbed water depth (h$_{i+1/2,j}$). The model automatically calculates the water/land boundary (Martin and Gorelick, 2005).

$$H_{i+1/2,j}^{N+1} = \max\left(0, h_{i+1/2,j} + \eta_{i,j}^{N+1}, h_{i+1/2,j} + \eta_{i+1,j}^{N+1}\right) \qquad (13)$$

$$H_{i,j+1/2}^{N+1} = \max\left(0, h_{i,j+1/2} + \eta_{i,j}^{N+1}, h_{i,j+1/2} + \eta_{i,j+1}^{N+1}\right) \qquad (14)$$

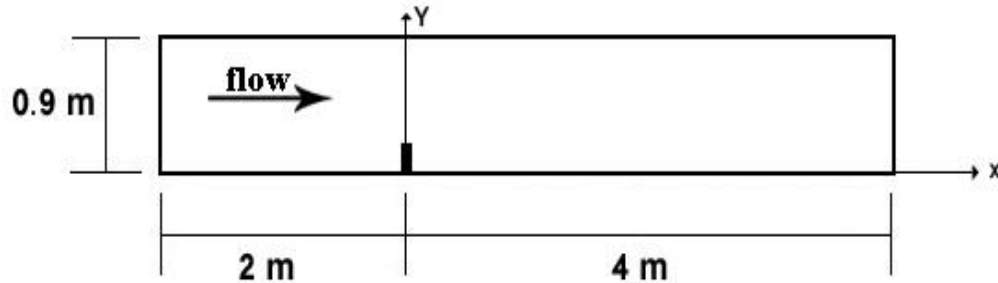Closed boundaries are boundaries that do not allow

Figure 3. Computational domain for simulation of Rajaratnam and Nwachukwu test case.

water flow while open boundaries are simulation domain boundaries which water may flow across them. Closed boundaries do not need specification in the proposed model because Equations 13 and 14 will determine the closed boundary locations in the simulation domain. However, open boundaries must be specified. Dirichlet boundary conditions were applied to inflow and outflow open boundaries.

VALIDATION OF PROPOSED MODEL

Rajaratnam and Nwachukwu test case

Rajaratnam and Nwachukwu (1983) conducted the experiments to study the characteristics of flow, near a thin plate groyne projected perpendicularly into a fully developed flow, in a long rectangular channel. The flume used in the experiments was 37 m long, 0.9 m wide and 0.76 m deep with smooth bed and sides. The groyne was an aluminum plate with 3 mm thickness and 152 mm length and was projected partly above the water surface. The flow velocity and water depth were U_0 = 0.253 m/s and H = 0.189 m, respectively. As shown in Figure 4, the resultant velocity profiles measured at y/l = 1.0, 1.5, 2.0, 3.0 and 4.0, where l = 152 mm is the length of the groyne, plotted after it was normalized by U_0 = 0.253 m/s and measured in upstream region.

Also, Quanhong and Pengzhi (2007) used from this experimental data to validate their model. Governing equations of their model were shallow water equations and depth-averaged k-ε model as the turbulence model. The results of these researchers model, in comparison with proposed model results, are presented as follows.

According to Quanhong and Pengzhi (2007) model shown in Figure 3, the computational domain is 6 m in length and 0.9 m in width. The upstream and downstream boundaries are located at 2 and 4 m away from the groyne respectively. Flow flux of 0.047817 m^2/s and water depth of 0.189 m is specified at the upstream and downstream boundaries respectively. As suggested by Molls et al. (1995), the horizontal eddy viscosity coefficient (ε = 0.0012 m^2/s) is adapted and assumed constant to be throughout the entire flow field. Also, the

Manning's roughness coefficient, n = 0.01 $s/m^{1/3}$ is assigned.

As shown in Figure 4, the agreement between experimental and computed results is satisfactory. The only major discrepancy occurs at y/b = 2, where the computed results under-predict the experimental data downstream of the groyne. This may be due to the very high velocity gradient arising in this region which makes the depth-averaged model inapplicable. Conversely, the experimental data may be erroneous in this region.

Holz (1990) test case

The laboratory experiments chosen for this section were conducted at the Franzius Institute, in Hannover, Germany. Velocity profiles were taken at 32.4 m long and 2.5 m wide horizontal concrete flume in which a 0.25 m long and 0.05 m wide groyne was placed perpendicular to the main flow. The computational domain chosen for the numerical experiments is shown in Figure 5, with which 6 monitor points are also shown. In these points, the horizontal velocity components at five depths (free surface, 0.2, 0.4, 0.6, 0.8 depths) were measured (Holz, 1990). The flow direction is from left to right and flow flux of 0.08 m^2/s and water depth of 0.23 m is specified at the upstream and downstream boundaries respectively. Also, horizontal eddy viscosity coefficient and Manning's roughness coefficient are like the previous test case.

Since the governing equations in this study are depth-averaged, shallow water equations, flow velocity of 0.6 depths was selected as the average velocity. Toro and Gomez (1998) also validated their three dimensional numerical model using the previous experimental results. The proposed model and Toro and Gomez model results, predict the flow depth around the groyne, these are shown in Figure 6. This figure shows that there are good agreements between the two models results.

Numerical tests performed show that, for uniform grid 0.05 × 0.05 m, the time step of 0.05 s provides desirable results. While the time step of Toro and Gomez model is more than three times smaller than the proposed model. This result shows that the proposed model efficiency is higher than Toro and Gomez model.
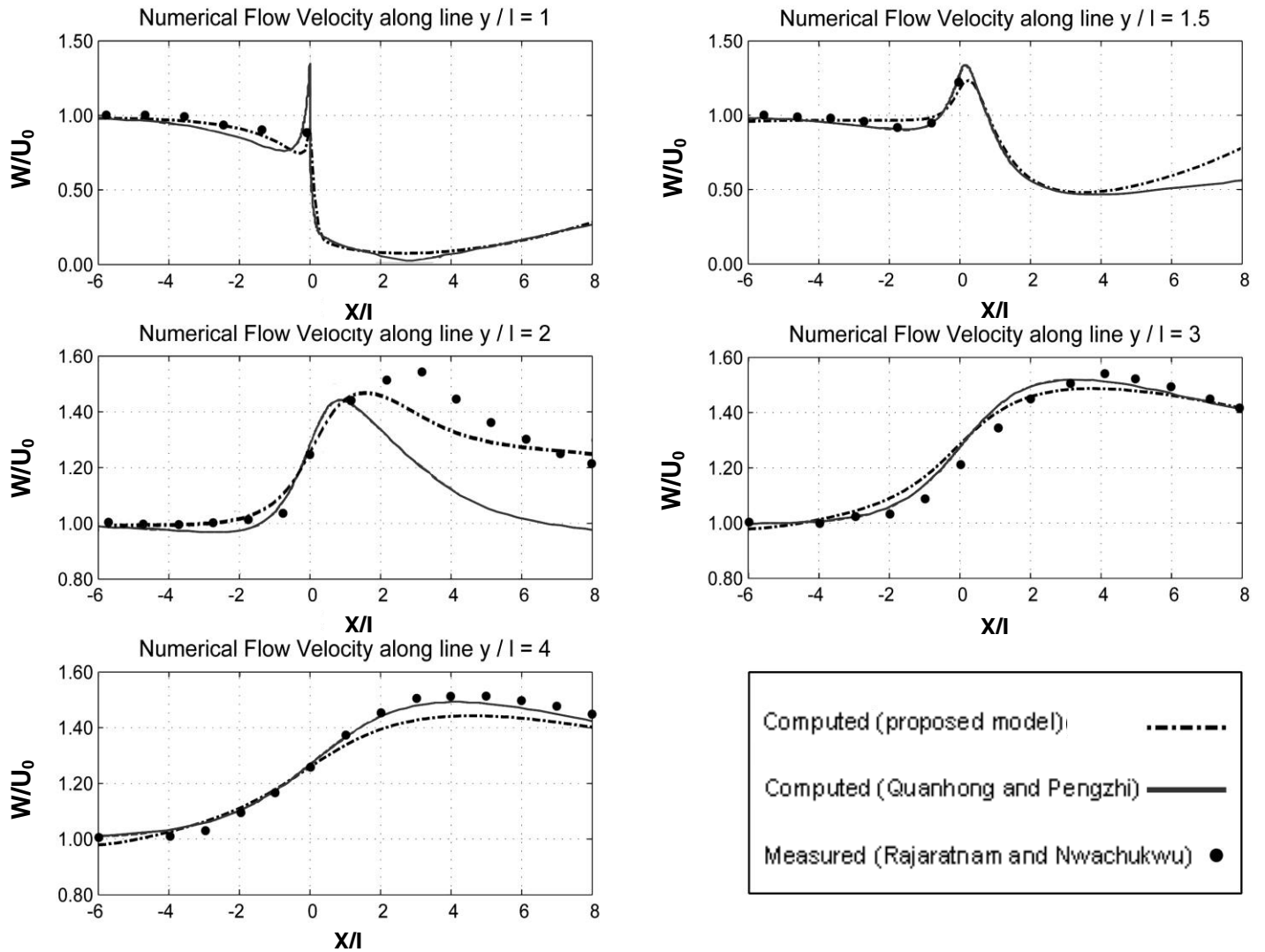
Figure 4. Comparison between resultant velocity profiles (W) of proposed model, Quanhong and Pengzhi model and Rajaratnam and Nwachukwu experimental data; all the velocities are normalized by $U_0 = 0.253$ m/s; x/l = 0 is the groyne position along flume direction.
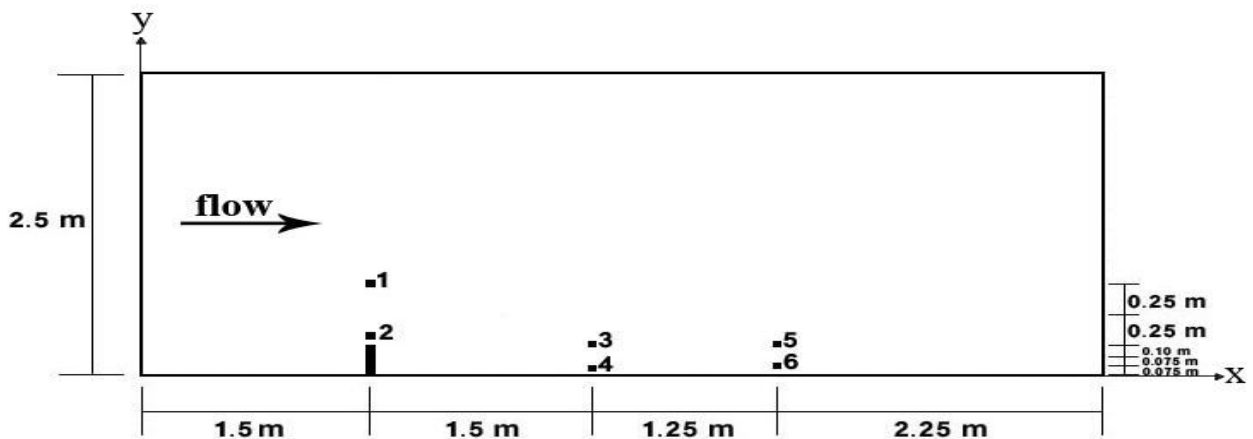

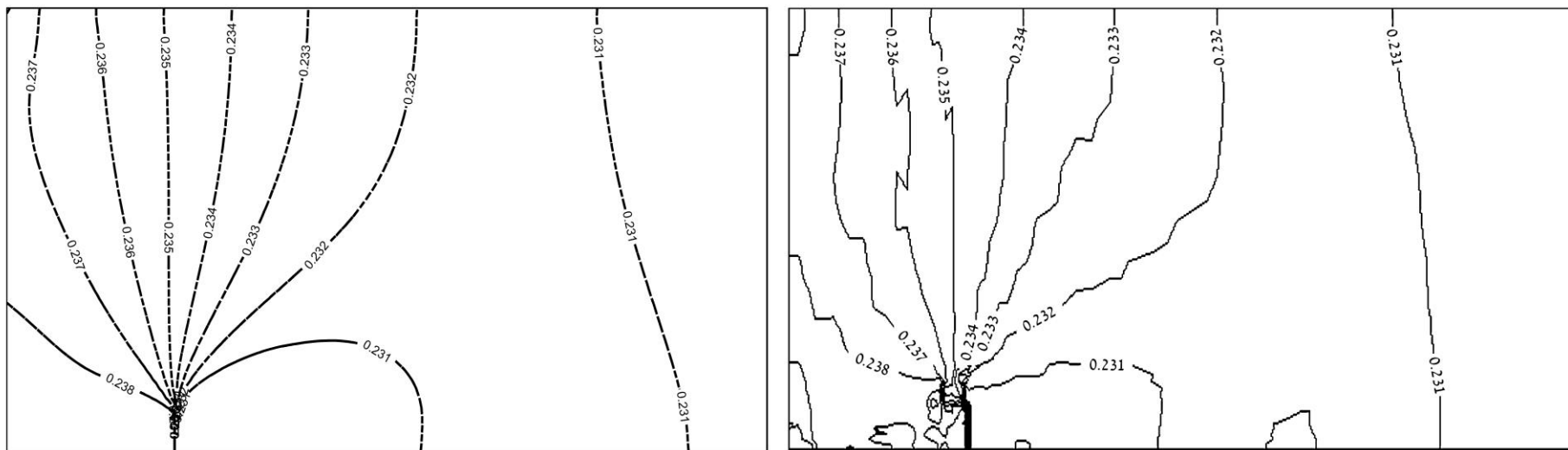**Figure 5.** Computational domain and monitor points for Holz test case.

Figure 6. Free surface elevation contours for test case 1, proposed model (left) and Toro and Gomez 3D model (right).

Table 1. The x and y velocity components (parallel to the channel walls and parallel to the dike axis, respectively) at the monitor points in the 60% flow depth from free surface.

Point	x velocity component (U)(m/s)			y velocity component (V)(m/s)		
	Proposed Model	Toro and Gomez 3D model	Experimental model	Proposed Model	Toro and Gomez 3D model	Experimental model
1	0.405	0.381	0.401	0.075	0.070	0.085
2	0.311	0.270	0.377	0.154	0.094	0.206
3	0.031	0.038	0.022	-0.003	-0.003	0
4	-0.087	-0.077	-0.095	0.002	0	0.017
5	0.166	0.176	0.150	-0.034	-0.025	-0.054
6	-0.015	0.039	-0.024	-0.014	-0.005	-0.018

Table 1 shows that at point 1 compared with point 2 which is farther from the groyne, both models have good agreement with experimental results. But at point 2, both numerical model results are not satisfactory. This aberration is due to the significant flow vertical component; however in shallow water equations it is negligible.

In monitor points that were placed in the downstream separation region of groyne (points 3 and 4) velocity components model have fairly good agreement with experimental results. Toro and Gomez model did not predict velocity components correctly in the point 6, because their model calculates the separation length incorrectly. But the proposed model present separation length
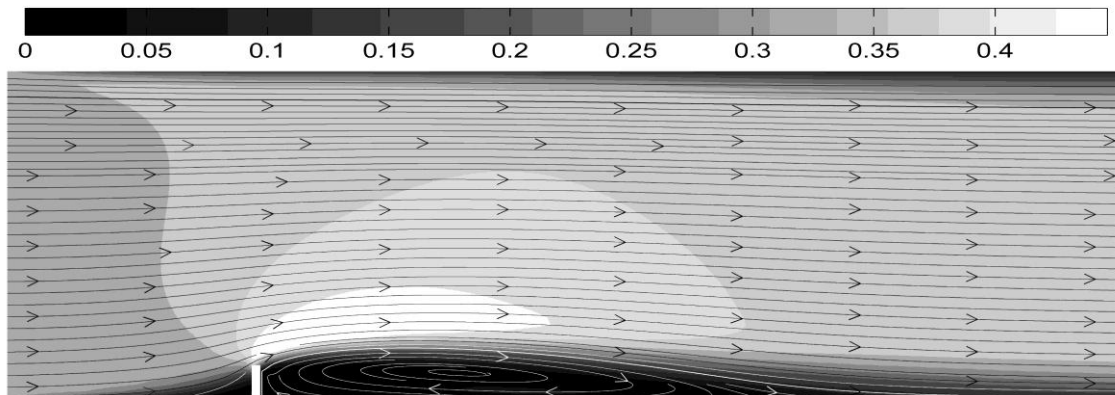
Figure 7. Streamline and flow velocity distribution around a groyne for test case 2.

(about 2.95 m) and velocity components properly. Also, Figure 7 shows streamline and flow velocity distribution around a groyne, which is obtained by the proposed model.

To determine the model's sensitivity towards Manning's roughness coefficient (n) and horizontal eddy viscosity coefficient (ε), these terms were varied and the results were compared. A change in the horizontal eddy viscosity coefficient (ε) and Manning's roughness coefficient (n) affected the final solution. An increase in each of the mentioned coefficients decreased the length of the recirculation zone, whereas decreasing these coefficients increased the recirculation length. Also, changing these coefficients affected the downstream velocities while the upstream velocities of the groyne remain relatively unaffected.

Finally, numerical tests showed that in the degree of implicitness of θ = 0.5, the proposed model is unstable. Although, the degree of implicitness θ = 1 obtains good accuracy but degree of implicitness θ = 0.8 provides the best results in terms of accuracy, stability and computational efficiency.

Conclusions

In this research, by combining a semi-implicit free surface solution and a semi-Lagrangian representation of advection, a very stable method for solving the shallow water equations is presented. Being free to take longer time-steps, due to high stability, allows a given forecast time to be reached with fewer steps. Two benefits were obtained from this. First, since fewer steps are taken, it is possible to reduce the total operation count for the forecast and a higher operational speed is gained. Secondly, by reducing the number of steps, the accumulated error may be reduced, therefore improves the forecast quality. Also, numerical representation has the ability to recognize land/water boundaries. Therefore, closed boundaries do not need specification. This capability especially in complex geometries can simplify the

solution algorithm and reduce the computational cost.

Numerical tests showed that the implicitness degree θ = 0.8, provides the best results in terms of accuracy, stability and computational efficiency. In order to validate the proposed model, the results that predict the flow pattern around the groyne, with numerical and experimental results of other researchers were compared.

The comparison between numerical formulation and experimental results showed that except in areas where strong downward flow is observed, there are good agreements between experimental and calculated results. Also, proposed model efficiency was higher than other presented numerical models.

REFERENCES

Abbasi S, Kamanbedast A, Ahadian J (2011). Numerical Investigation of Angle and Geometric of L-Shape Groin on the Flow and Erosion Regime at River Bends. World Appl. Sci. J., 15(2): 279-284.

Bermejo R (1990). On the equivalence of semi-lagrangian schemes and particle-in-cell finite element methods. Monthly Weather Rev., 118: 979-987.

Chunmiao Z, Bennett GD (1995). Applied contaminant transport modelling: theory and practice. Van Nostrand Reinhold New York. pp. 235-387.

Clive AJ (1991). Computational Techniques for Fluid Dynamics: Volume I, volume I of Springer Series in Computational Phys. Springer-Verlag Berlin second edition, p. 53.

Ettema R, Muste M (2004). Scale Effects in Flume Experiments on Flow around a Spur Dike in Flatbed channel J. Hydraulic Eng., 130: 635-646.

Francis JR, Pattanick A, Wearne S (1968). Observations of flow patterns around some simplified groyne structures in channels. Technical Note No. 8. Proc. Inst. Civil Eng. London. England, pp. 829-846.

Holz (1990). Numerical Simulation of Three-Dimensional Turbulent Flow in Harbor Entrances and Navigation Channels.Technical Report. Volskwagenwerk Foundation.

Hestenes MR, Stiefel E (1952). Method of Conjugate Gradients for Solving Linear Systems. J. Res. Natl. Bur. Stand., 49(6): 409-436.

Leonard BP (1993). Positivity-preserving numerical schemes for multidimensional advection. Technical Report ICOMP-93-05, Institute for Computational Mechanics in Propulsion, p. 27.

Martin N, Gorelick M (2005). A MATLAB surface fluid flow model for rivers and streams. Comput. Geosci. 31: 921-94.

Molls T, Chaudhry MH, Khan KW (1995). Numerical simulation of two-

dimensional flow near a spur dike. J. Advance in Water Res., 118(4): 227-236.

Quanhong L, Pengzhi L (2007). Numerical Simulation of Recirculating Flow Near a Groyne. The 2nd International Conference on Marine Research and Transportation. Ischia. Naples. Italy, pp. 61-68.

Robert A (1982). A Semi-Lagrangian, semi-implicit numerical integration scheme for primitive meteorological eguation. Atmos-Oceans, 19: 35-46.

Rajaratnam N, Nwachukwu BA (1983). Flow near Groin-like structures, J. Hydraulic Eng. ASCE, 109(3): 463-480.

Shahrokhi M, Sarveram H (2011). Three-Dimensional Simulation of Flow around a Groyne with Large Eddy Turbulence Model. JFAE, 9(3&4): 132-136.

Staiforth A, Cote J (1991). Semi-Lagrangian integration schemes for atmospheric models-a review. Mon. Weather Rev., 119(9): 2206-2223.

Toro B, Gomez G (1998). A Semi-Implicit 3D Numerical Model for Free Surface Flows. Parallel Session (parallel56). Numerical Methods for Current and Wave Calculation, pp.1-26.

Tingsanchali T, Maheswaran S (1990). 2-D Depth-Averaged Flow Computation Near a Groyne. J. Hydraulic Eng. ASCE., 116(1): 71-96.

Tang X, Ding X (2007). Experimental and Numerical Investigation on Secondary Flows and Sedimentions Behind a Spur Dike. J. Hydrodynamics. Ser., B, 19(1): 23-29.

Vicenzo CV (1990). Semi-implicit finite difference methods for the two dimensional shallow water equations. J. Comput. Phys., 86: 56-74.

Yeo HK, Kang JG, Kim SJ (2005). An Experimental Study on Tip Velocity and Downstream Recirculation Zone of Single Groyne of Permeability change. KSCE J. Civil Eng., 9(1): 29-38.

Zhanfeng C, Xiaofeng Z (2006). Flow and Sediment Simulation Around Spur Dike With Free Surface Using 3-D Turbulent Model. Conference of Global Chinese Scholar on Hydrodynamics, Shanghai, China, pp. 237-244.